ISSN 0023-1584, Kinetics and Catalysis, 2018, Vol. 59, No. 2, pp. 143–149. © Pleiades Publishing, Ltd., 2018.
Original Russian Text © T.A. Bugrova, G.V. Mamontov, 2018, published in Kinetika i Kataliz, 2018, Vol. 59, No. 2, pp. 169–176.

The Study of CrO_x-Containing Catalysts Supported on ZrO_2, CeO_2, and $Ce_xZr_{(1-x)}O_2$ in Isobutane Dehydrogenation[1]

T. A. Bugrova* and G. V. Mamontov

National Research Tomsk State University, Tomsk, 634050 Russia

**e-mail: bugrova.tatiana@gmail.com*

Received January 31, 2017

Abstract—Olefin hydrocarbons are valuable raw materials for petrochemical and polymer manufacturing. Highly effective, but toxic chromium-containing catalytic materials are the most widely used catalysts to obtain olefins in industry. In this regard, the urgent challenge to increase the efficiency of oil processing is to develop the catalysts with low content of harmful active component. In the present study, the catalysts with low chromium content (1 theoretical monolayer = 5 Cr atoms per nm^2 of support) were synthesized by incipient wetness impregnation of the supports (Al_2O_3, ZrO_2, CeO_2, and $Ce_xZr_{(1-x)}O_2$). The samples obtained were characterized by low-temperature nitrogen adsorption, X-ray diffraction and H_2-temperature-programmed reduction methods. The catalytic properties of the catalysts were tested in isobutane dehydrogenation reaction. It was shown that the state of chromium on the surface is different over different supports. For the CrO_x/CeO_2 catalyst, the formation of Cr_2O_3 particles with low activity in the dehydrogenation reaction was observed. For other samples, a highly disperse X-ray amorphous state of chromium was characteristic. The catalyst based on $Ce_xZr_{(1-x)}O_2$ was the most active in isobutane dehydrogenation reaction due to possible stabilization of chromium as Cr(V) state.

Keywords: Cr-containing catalysts, ZrO_2, CeO_2, $Ce_xZr_{(1-x)}O_2$, isobutane dehydrogenation

DOI: 10.1134/S0023158418020027

INTRODUCTION

Olefin hydrocarbons (ethylene, propylene, isobutylene, etc.) are valuable chemical compounds for the production of polymers, dyes, rubbers, fibrous materials, etc. They are mainly formed as by-products in the processes of steam cracking of naphtha and catalytic cracking of heavy oil fractions. These alkenes are also produced in a large scale by dehydrogenation of the corresponding alkanes. At present, the catalytic nonoxidative dehydrogenation (DH) of paraffinic hydrocarbons is of great industrial importance and is a large-scale petrochemical process. The most widely used catalysts for DH of C_3–C_5 alkanes are those containing Pt–Sn or CrO_x supported on Al_2O_3 [1–3]. However, the use of such systems is limited due to high cost of platinum and the toxicity of chromium oxides. Thus, various types of supported and bulk oxides (indium [4], vanadium [5, 7], gallium [8, 9] and molybdenum [10] oxides) are studied to obtain alternative catalysts for hydrocarbon dehydrogenation possessing comparable properties to Pt- and Cr-containing ones. Nevertheless, in the review by Sattler J.J.H.B. et al. [11] concerning modern state of research of such systems (namely, deposited gallium, vanadium and molybdenum oxides) for oxidative and non-oxidative dehydrogenation of hydrocarbons, the authors concluded that these catalysts are significantly inferior to chromium- and platinum-containing systems, rapidly deactivate and lose activity after the regeneration stage. Carrying out the oxidative dehydrogenation in the presence of O_2 and/or CO_2 leads to the partial and deep oxidation of hydrocarbons and selectivity loss. Therefore, the development of chromium-containing systems with high catalytic activity even at low content of the active component is the up-to-date direction of scientific research.

γ-Al_2O_3 [12–14], SiO_2 [15, 16], ZrO_2 and TiO_2 [5, 17, 18], zeolites [19], MgO [20], ordered mesoporous materials [21, 22], etc., were studied as supports for chromium-containing catalysts. It is known that the state of active component in the catalyst and its efficiency are determined by support properties, conditions of catalyst synthesis and the addition of modifiers/promoters of various nature. The change of some parameter allows controlling the state of active phase. γ-Al_2O_3 is widely used as a support for chromium-containing systems. CrO_x-catalysts based on ZrO_2 even with low content of the active component are the most active in the dehydrogenation of hydrocarbons [23, 24]. However, their use is limited by high price of zirconium compounds, the complexity to

[1] The article was translated by the authors.

obtain a support with a developed specific surface area and sintering at high temperatures [25]. Chromium-containing systems may differ in terms of the amount of chromium introduced as well as the nature of the precursor, composition, conditions of preparation and subsequent treatment, and the state of the oxide support surfaces. Nevertheless, on the surfaces of both alumina and zirconia, a significant part of chromium is in a highly dispersed Cr(VI) state due to possible strong interaction of chromium ions with the surface of ZrO_2 or Al_2O_3 that prevents their segregation into the low-active phase of α-Cr_2O_3. Zircona and other oxides (SiO_2, La_2O_3, etc. [26–29]) are also used as modifiers in CrO_x/Al_2O_3 catalysts. According to the literature data, it is possible to estimate the state of chromium oxides on the surface of various supports and approach the understanding of the mechanisms of active phase formation. Nevertheless, despite increasing attention to CeO_2, CeO_2-containing materials and mixed oxides of $Ce_xZr_{(1-x)}O_2$ as catalysts, modifiers and supports for various applications, the studies focused on application of cerium-containing materials in dehydrogenation processes are limited mainly by reactions in the oxidative mode [30]. However, the systems that contain ceria as a modifier or support can be of interest because of the ability of CeO_2 to increase the dispersion of the active component (in particular, Cr, W, V oxides) in calcined samples by forming surface states M–O–Ce [31–33].

The purpose of the present work was to study the state of chromium deposited on CeO_2 and $Ce_xZr_{(1-x)}O_2$, in comparison with Al_2O_3- and ZrO_2-based catalysts and the catalytic properties of the obtained model chromium-containing samples in the isobutane dehydrogenation reaction.

EXPERIMENTAL

Synthesis of Supports and Catalysts

γ-Al_2O_3, ZrO_2, CeO_2 and $Ce_xZr_{(1-x)}O_2$ were used as supports. Aluminum, cerium and zirconium oxides were obtained by thermal decomposition of AlO(OH), $Ce(NO_3)_3 \cdot 6H_2O$ and $ZrO(NO_3)_2 \cdot H_2O$, respectively, at 600°C for 4 h. Since γ-Al_2O_3 is a classical and the most commonly used support for chromium-containing catalysts, it was used for comparison with the catalysts based on other supports. Mixed $Ce_xZr_{(1-x)}O_2$ oxide was synthesized by co-precipitation method. The calculated amounts of $Ce(NO_3)_3 \cdot 6H_2O$ and $ZrO(NO_3)_2 \cdot H_2O$ (Ce : Zr molar ratio = 1 : 1) were dissolved in distilled water, and then an aqueous solution of ammonia $NH_3 \cdot nH_2O$ (2 mol/L) was added dropwise. The precipitate was dried at 90°C for 12 h and calcined at 500°C for 4 h.

Model Cr-containing catalysts were prepared by incipient wetness impregnation of the obtained supports with an aqueous solution of CrO_3 (reagent grade). The chromium content corresponded to one monolayer (5 Cr atoms per nm^2 of support) [23] that was 2–8 wt % of Cr. The synthesized catalysts were dried at 95°C for 12 h, calcined in air atmosphere at 600°C for 4 h.

Characterization of Supports and Catalysts

The measurement of porous structure characteristics of the materials was carried out by low-temperature nitrogen adsorption at –196°C using TriStar 3020 automated gas adsorption analyzer (Micrometritics, USA). The specific surface area was determined by the multipoint BET method via linearization of the adsorption isotherm in the P/P_0 range from 0.05 to 0.30. The Barrett–Joyner–Halenda method (BJH-Desorption) with an analysis of the desorption branch of the nitrogen adsorption–desorption isotherm was used to plot the pore size distribution. The samples (100–120 mg) were degassed in vacuum at 200°C for 2 h prior to the measurements.

Diffuse reflectance spectroscopy (DRS or UV-vis spectroscopy) and X-ray diffraction (XRD) methods were used to study the chemical state of chromium and the phase composition of the catalysts. Diffuse reflectance spectra were recorded on a Cary spectrometer (Varian, Australia) with DRA-CA-30I attachment (Labsphere, USA) in the wavelength range of 250–800 nm. MgO was used as a standard sample. XRD patterns were obtained on a Miniflex 600 diffractometer (Rigaku, Japan) using monochromatic CuK_α radiation (λ = 1.5418 Å) with a scanning rate of 0.2 deg/min, step size of 0.2 deg and 2θ = 10°–90°. The phase composition of the catalysts was determined using the PCPDFWIN database and the POWDER CELL 2.4 full profile analysis software.

Temperature-programmed reduction with hydrogen (TPR-H_2) was carried out using ChemiSorb 2750 chemisorption analyzer (Micromeritics, USA) equipped with thermal conductivity detector (TCD). The experiments were carried out at a heating rate of 10°C/min using a 10 vol % H_2/Ar mixture with a flow rate of 20 mL/min.

To calculate the amount of weakly bound Cr(VI), the catalysts were boiled in distilled water according to the method described in [34]. Chromium amount in soluble form was determined by inductively coupled plasma mass spectrometry (ICP-MS) method using Agilent 7500c spectrometer (Agilent, USA).

Catalytic Tests

The activity of the prepared catalysts was investigated in the reaction of isobutane dehydrogenation in a tubular quartz flow reactor with a fixed catalyst bed at 540°C. The reaction mixture (15% i-C_4H_{10}/N_2) was passed through the catalyst bed (V_{cat} = 0.75 mL, particle size was 0.25–0.5 mm) diluted with quartz glass

with a flow rate of 9 L/h (12000 h^{-1}). A test was carried out for 1 h with the product gas sampling for the first analysis at sixth minute, then the sampling was carried out every 12 min. The gaseous products of the reaction were analyzed on Chromatec Crystall 5000.2 gas chromatograph (Chromatec, Russia) with a thermal conductivity detector (TCD) and two flame ionization detectors (FID). The components formed during the dehydrogenation (saturated and olefinic hydrocarbons C_1–C_4) were separated using a Capillary Column CP-Al_2O_3/Na_2SO_4 (Varian, Australia, 50 m, 130°C). The Chromatec Analytic 2.6 software was used for quantitative determination of the components of the gas mixture according to absolute calibration method involving the use of calibration gas mixture. The mixture was standardized according to the Primary Standard GET 154 2001 (the RF State Standard GOST 8.578-2002 concerning gas standardization).

RESULTS AND DISCUSSION

Characterization of Catalysts

The porous structure of the synthesized supports and catalysts on the basis thereof was investigated using the low-temperature nitrogen adsorption. Figure 1 shows nitrogen adsorption–desorption isotherms and pore size distribution for supports Al_2O_3, CeO_2, ZrO_2 and $Ce_xZr_{(1-x)}O_2$ and Cr-containing catalysts. The presence of a hysteresis loop indicates the mesoporous structure of all supports and catalysts. Aluminum oxide and the catalyst on the basis thereof are characterized by a hysteresis loop in the range of relative pressure from 0.46 to 1.0. One can see from the pore size distribution (Fig. 1a) that the porous structure of Al_2O_3 and CrO_x/Al_2O_3 samples is represented by small (2–5 nm) and medium (5–30 nm) mesopores. The nitrogen adsorption–desorption isotherm for CeO_2, ZrO_2 and $Ce_xZr_{(1-x)}O_2$ have a hysteresis loop in the range of relative pressure of 0.65–1 (ZrO_2), 0.67–1 (CeO_2) and 0.4–1 ($Ce_xZr_{(1-x)}O_2$). These values also correspond to mesoporous structure. However, the porous structures of the CeO_2, ZrO_2 and $Ce_xZr_{(1-x)}O_2$ differ from the one of Al_2O_3. The porous structures of zirconium, cerium and mixed cerium–zirconium oxides mainly contain the pores with sizes of 5–35, 2–25 and 2–7 nm, respectively.

The values of specific surface area (S_{BET}), pore volume (V_{pore}) and pore diameter (D_{pore}) for catalysts and supports are presented in Table 1. Alumina support has a specific surface area of 201 m^2/g, a total pore volume of 0.24 cm^3/g, and an average pore diameter of 6.3 nm. The corresponding values for ZrO_2 and CeO_2 are 47 m^2/g, 0.24 cm^3/g , 16.3 nm and 84 m^2/g, 0.23 cm^3/g and 9.1 nm, respectively. $Ce_xZr_{(1-x)}O_2$ support is the most fine-pored with the specific surface area of 52 m^2/g, pore volume of 0.03 cm^3/g and an average pore diameter of 3.1 nm. Thus, the porous structure of the obtained supports differs significantly.

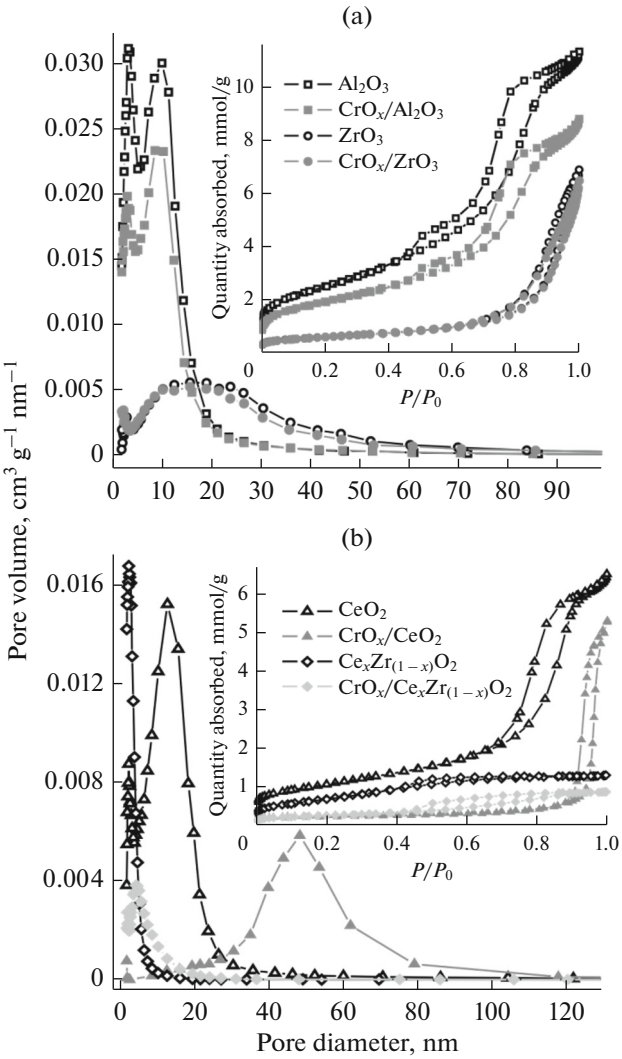

Fig. 1. Nitrogen adsorption–desorption isotherms (a) and pore size distribution (b) for supports and catalysts.

A decrease of specific surface area and pore volume are observed for chromium-containing catalysts in comparison with the initial supports. The ZrO_2-supported catalyst is an exception due to mutual influence of CrO_x and zirconia. ZrO_2 support stabilizes the active component in a highly dispersed state, while chromium oxide suppresses sintering of zirconia at high temperatures [24].

Porous structure of CrO_x/CeO_2 and $CrO_x/Ce_xZr_{(1-x)}O_2$ samples differs significantly from those of CeO_2 and $Ce_xZr_{(1-x)}O_2$ (Fig. 1b). The values of specific surface area for CrO_x/CeO_2 and $CrO_x/Ce_xZr_{(1-x)}O_2$ catalysts are 19 and 20 m^2/g, respectively, while the size of pores increases significantly: 9.1 nm (CeO_2) and 29.7 nm (CrO_x/CeO_2). The

Table 1. Characteristics of supports and catalysts

Sample	S_{BET}, m^2/g	V_{pore}, cm^3/g	D_{pore}, nm*	Sample	S_{BET}, m^2/g	V_{pore}, cm^3/g	D_{pore}, nm*
Al_2O_3	201	0.40	6.3	CrO_x/Al_2O_3	154	0.31	6.8
ZrO_2	47	0.24	16.3	CrO_x/ZrO_2	47	0.23	16.2
CeO_2	84	0.23	9.1	CrO_x/CeO_2	19	0.18	29.7
$Ce_xZr_{(1-x)}O_2$	52	0.03	3.1	$CrO_x/Ce_xZr_{(1-x)}O_2$	20	0.04	5.5

* BJH-desorption method.

change of porous structure can be explained by interaction of chromic acid with cerium oxide during the impregnation step followed by the growth of CeO_2 particles during the calcination.

XRD patterns of the synthesized chromium containing catalysts and supports are presented in Fig. 2. Only reflexes of support phases were observed for the catalysts based on Al_2O_3, ZrO_2 and $Ce_xZr_{(1-x)}O_2$: γ-Al_2O_3 [26] phase, in monoclinic and tetragonal modifications of zirconium oxide phases [24]; phases of $(Ce,Zr)O_2$ mixed oxide and tetragonal ZrO_2, respectively. The presence of tetragonal modification of ZrO_2 in the $Ce_xZr_{(1-x)}O_2$ is caused by possible formation of oxygen vacancies to compensate the charge or due to distortion of the ZrO_2 lattice. After detailed analysis of XRD patterns in the range of 2θ = 20°–38°, the reflexes of α-Cr_2O_3 phase (2θ = 24.50°, 33.61° and 36.20°) and other chromium-containing phases, which can overlap with the reflexes of ZrO_2 and Al_2O_3 phases, were not found. This indicates a highly dispersed X-ray amorphous state of chromium.

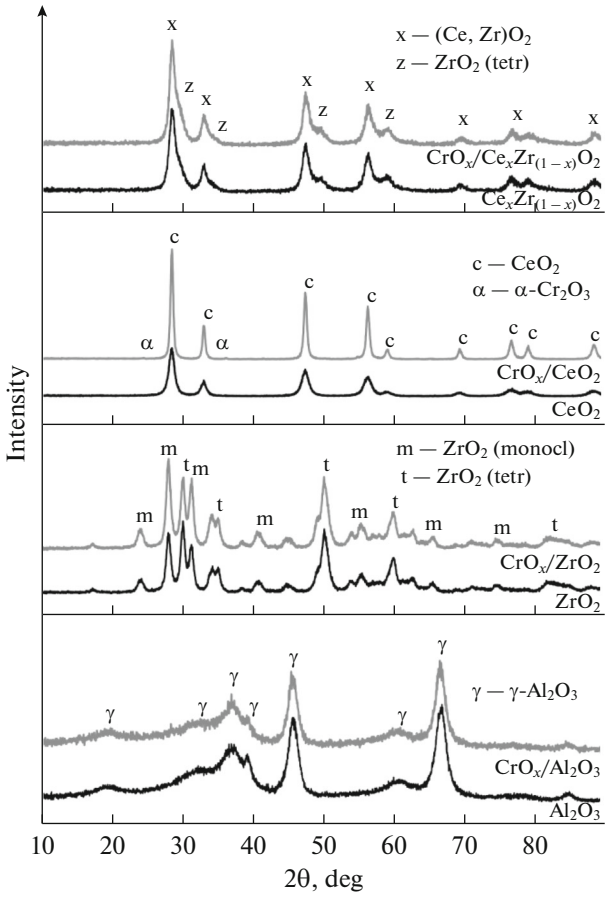

Fig. 2. X-ray diffraction patterns of supports and catalysts.

Contrary to other catalysts, the XRD pattern of CrO_x/CeO_2 catalyst contains both reflexes of support phase (CeO_2) and those of α-Cr_2O_3 phase at 2θ = 24.50° and 36.20° (Fig. 3 shows enlarged fragment of the pattern for CrO_x/CeO_2 catalyst in the range from 21° to 39°). The presence of reflexes of chromium oxide phase is caused by the possible interaction of the chromic acid with the support during the impregnation step. An increase of intensity of CeO_2 reflexes is also observed in comparison with the support and is caused by agglomeration of the particles during the reprecipitation and calcination. The size of the CeO_2 crystallites for initial support (according to the Scherer equation) is 5.9 nm, while the value for the catalyst is 18.3 nm.

Figure 4 shows the DRS spectra of the catalysts. In the spectra of all catalysts, the absorption bands/shoulders with maximums at 276 and 380 nm indicate the presence of chromium mainly in a Cr(VI)

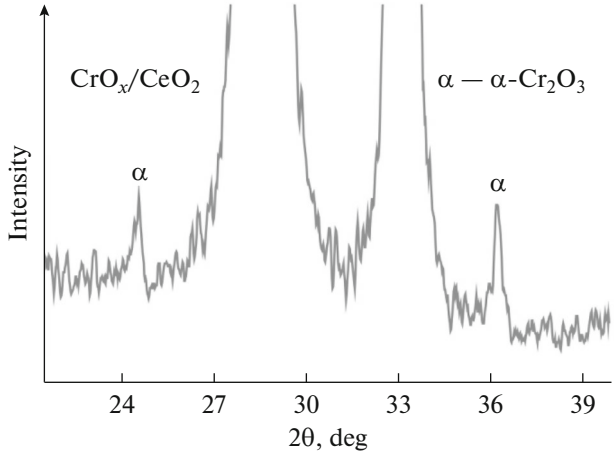

Fig. 3. X-ray diffraction pattern of CrO_x/CeO_2 in the range of 2θ = 21°–39°.

state (with tetrahedral coordination) [34]. In spectra of CrO_x/CeO_2 sample, the doublet in the visible region with maximums at 468 and 598 nm is associated with chromium in a Cr(III) state of α-Cr_2O_3 (octahedral coordination) [3, 23, 35], which correlates with the XRD results. The band with maximum at 701 nm also corresponds to *d*–*d*-transition of Cr^{3+} cations in octahedral oxygen coordination according to [34]. The shoulder at 719 nm is observed in the DRS spectra of the catalyst supported on $Ce_xZr_{(1-x)}O_2$, but the doublet in the range that corresponds to Cr^{3+} state was not found. However, the presence of a shoulder at 532 nm along with the band at 731 nm probably indicates chromium as Cr^{5+} [36]. It is noteworthy that up to 50% of chromium can be stabilized as mononuclear Cr(V) sites on the ZrO_2 surface at small chromium content (less than 1 monolayer) according to the results obtained in Ref. [23]. This chromium state can be found mainly by the ESR method. It is believed that the mononuclear Cr(V) sites form isolated Cr^{3+} sites upon reduction, which are the most active in the dehydrogenation of paraffinic hydrocarbons.

Figure 5 shows the TPR-H_2 profiles for the supports and Cr-containing catalysts. Hydrogen consumption peak in the temperature range of 260–450°C is attributed to reduction of $Cr^{VI}O_x$ and/or $Cr^{V}O_x$ to Cr_2O_3 [3, 37]. The peaks at 515 and 590°C for CrO_x/CeO_2, $CrO_x/Ce_xZr_{(1-x)}O_2$ are associated with reduction of the supports. A shift of hydrogen consumption peak in the low-temperature range for CrO_x/ZrO_2 sample is probably connected with high fraction of Cr^{V}, higher dispersion of chromium oxides on the ZrO_2 surface or weak interaction of active component with the support. An increase of reduction temperature of CrO_x species for CrO_x/CeO_2 and $CrO_x/Ce_xZr_{(1-x)}O_2$ catalysts are caused by possible interaction between the precursor of active component and CeO_2 in the course of impregnation procedure. This interaction leads to formation of larger chromium oxide particles, which are able to participate in reversible oxidation–reduction, or oxide particles that interact stronger with the support in comparison with the ZrO_2-based catalysts.

The amount of hydrogen consumed according to reaction $2CrO_3 + 3H_2 = Cr_2O_3 + 3H_2O$ calculated from the areas of TPR-H_2 peaks (after deduction of hydrogen consumed for reduction of supports) are presented in Table 2. It can be seen that CrO_x/CeO_2 catalyst is characterized by the lowest fraction of Cr^{VI} (22.5%) transforming into Cr^{III} state during the reduction. The Cr^{III} state provides the activity of the catalysts in the dehydrogenation reaction. The remaining part of active component is presented by the particles of α-Cr_2O_3 phase that is not able to reduce under mentioned conditions according to UV-vis DRS and XRD (Figs. 2–4). The highest content of Cr^{VI} is observed for

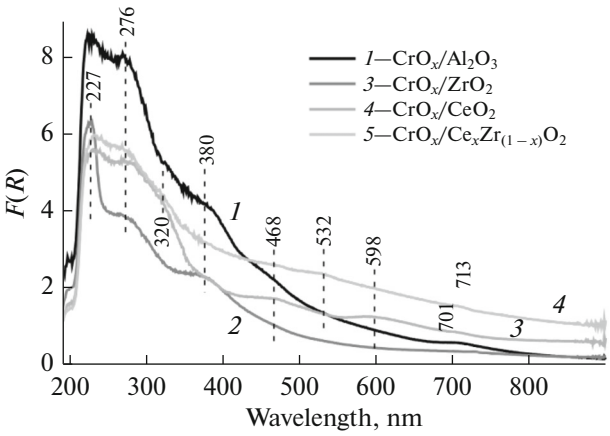

Fig. 4. DRS spectra of the synthesized chromium-containing catalysts.

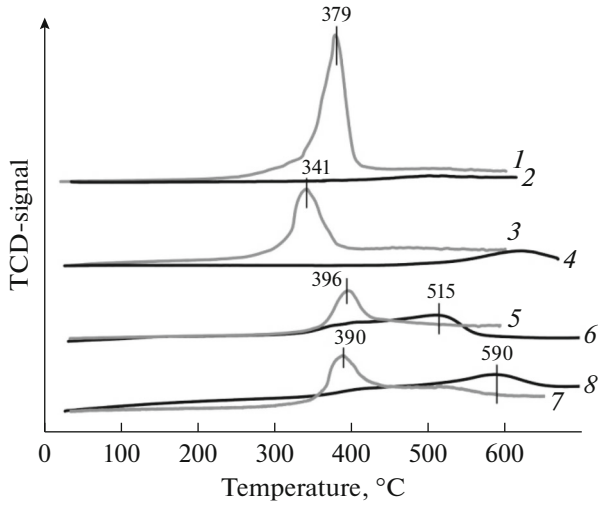

Fig. 5. TPR-H_2 profiles of reduction of supports and catalysts: (*1*) CrO_x/Al_2O_3, (*2*) Al_2O_3, (*3*) CrO_x/ZrO_2, (*4*) ZrO_2, (*5*) CrO_x/CeO_2, (*6*) CeO_2, (*7*) $CrO_x/Ce_xZr_{(1-x)}O_2$, (*8*) $Ce_xZr_{(1-x)}O_2$.

CrO_x/ZrO_2 (66.1%) and $CrO_x/Ce_xZr_{(1-x)}O_2$ (62.3%) catalysts. This indicates the ability of ZrO_2 to stabilize chromium in a high-valence states. Table 2 additionally shows the data on the fraction of weakly bound Cr^{VI} obtained by ICP–MS analysis of the solution after boiling of the catalysts in water depending on total chromium content. Estimation of the amount of strongly bound and soluble forms of Cr^{VI} revealed that the content of strongly bound form is higher than the soluble one for all samples. From the results presented in Table 2 we can conclude that the Cr^{VI} fraction in the catalysts is mainly determined by the amount of strongly bound Cr^{VI}, which depends on the strength of "active component–support" interaction. The content of water-soluble Cr^{VI} species is the largest for CrO_x/γ-Al_2O_3 catalyst (14.4%). The amount of strongly bound

Table 2. Properties of catalysts

Catalyst	Cr, wt %	$D_{Cr_2O_3}$, nm	Cr(VI) part, %*	Fraction of weakly bound Cr(VI), %**	Fraction of strongly bound Cr(VI), %
$CrO_x/\gamma\text{-}Al_2O_3$	8.0	–	35.3	14.4	20.9
CrO_x/ZrO_2	2.0	–	66.1	12.5	53.3
CrO_x/CeO_2	3.5	6.7	22.5	3.4	19.1
$CrO_x/Ce_xZr_{(1-x)}O_2$	2.2	–	62.3	5.6	56.7

* TPR data (without taking into account the possible presence of Cr(V) in the catalyst).

** ICP–MS data.

The dashes mean that the reflexes of Cr_2O_3 phase were not observed.

Cr^{VI} for CrO_x/ZrO_2 and $CrO_x/Ce_xZr_{(1-x)}O_2$ catalysts (53.3 and 56.7%, respectively) is significantly higher than the one of weakly bound species that may be caused by stronger interaction of chromium with ZrO_2 and $Ce_xZr_{(1-x)}O_2$. Thus, the chromium state on the catalysts surface significantly depends on the support nature.

Catalytic Activity

Catalytic properties of the prepared Cr-containing catalysts were investigated in the isobutane dehydrogenation without reductive pretreatment before the dehydrogenetion reaction. Figure 6 shows the dependencies of catalytic activity on the reaction time (from 6 to 66 min). The $CrO_x/Ce_xZr_{(1-x)}O_2$ catalyst possesses the highest specific activity (mmol(i-C_4H_{10}) m^{-2} h^{-1}). It is noteworthy that ZrO_2-based catalyst demonstrated the best catalytic performances after the first sampling at 6th min of the dehydrogenation reaction. However, this catalyst underwent the fast deactivation due to coke deposition on the surface. The amount of coke on the surface of the CrO_x/ZrO_2 catalyst after the 66th minute of dehydrogenation reaction followed by cooling in the inert atmosphere (nitrogen) was 2.26 wt % according to simultaneous thermal analysis data (TG–DSC). The CrO_x/CeO_2 is the most stable catalyst during the dehydrogenation process [24]. Preparation of the catalyst on the basis of mixed Ce–Zr oxides allows combining the stability of the CeO_2- and ZrO_2-supported catalysts. Comparing the results of investigation of chromium chemical state and catalytic properties of the prepared Cr-containing catalysts, it can be concluded that CrO_x species on the surface of CrO_x/ZrO_2 and $CrO_x/Ce_xZr_{(1-x)}O_2$ catalysts were highly dispersed (amorphous state) according to the UV-visible DRS and XRD data. Moreover, the mentioned samples contain more than 60% of Cr^V and Cr^{VI} (fraction from total amount of chromium in the catalyst) according to the TPR-H_2 data. Large part of Cr^{VI} was presented by $Cr^{VI}O_x$ species strongly bound to the surface. Highly dispersed amorphous particles of Cr^{III} oxide provided high activity of the catalyst in the isobutane dehydrogenation and formed during the reduction of $Cr^{VI}O_x$ species. The $\alpha\text{-}Cr_2O_3$ particles possessing low activity in the isobutane dehydrogenation appeared on the surface of CeO_2 due to the interaction of the support and the precursor of active component. The $CrO_x/\gamma\text{-}Al_2O_3$ catalyst is characterized by the lowest activity in spite of the fact that the fractions of reducible Cr^{VI} were higher than those in CrO_x/CeO_2 (35.3 and 22.5%, respectively). This may be caused by higher activity of chromium species that can be reduced to Cr^{III} on the surface of ZrO_2, $Ce_xZr_{(1-x)}O_2$ and CeO_2 in comparison with those over $\gamma\text{-}Al_2O_3$ [38]. Thus, according to [35], the Cr^{III} species formed during the reduction of soluble forms of Cr^{VI} sites were the most active and selective. On the other hand, it was proposed that the isolated Cr^{III} sites formed during the reduction of mononuclear Cr^V species are the most active in dehydrogenation of hydrocarbons [23]. High activity of the CrO_x/ZrO_2 and $CrO_x/Ce_xZr_{(1-x)}O_2$ catalysts may be also associated with the presence of these sites that are strongly bound to the support surface.

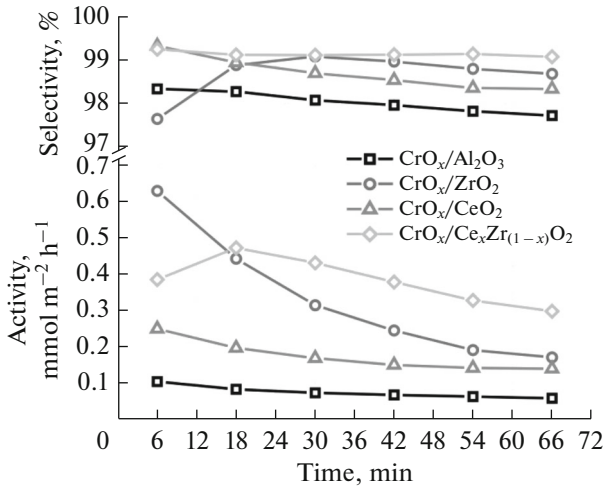

Fig. 6. Time dependence of activity of the catalysts in isobutane dehydrogenation and selectivity towards isobutylene.

CONCLUSIONS

Thus, the catalysts based on ZrO_2 and $Ce_xZr_{(1-x)}O_2$ supports showed the highest activity in the reaction of isobutane dehydrogenation in spite of low specific surface area of these supports. The interaction of CeO_2 with CrO_x precursor and formation of particles of α-Cr_2O_3 phase was found for CrO_x/CeO_2 system. The formation of CrO_x species that are able to reduction, but less active in dehydrogenation reaction was observed for chromia–alumina catalysts. It was shown that the surface of ZrO_2 and $Ce_xZr_{(1-x)}O_2$ was capable to stabilize the active component (with its small content) in a strongly bound, highly dispersed amorphous state. This state determined the high activity of the catalyst in the isobutane dehydrogenation.

ACKNOWLEDGMENTS

The authors thank A.V. Livanova for XRD studies and Dr. E.D. Fakhrutdinova for DRS studies. This work was supported by "The Tomsk State University Academic D. I. Mendeleev Fund Program" grant in 2018.

REFERENCES

1. Rashidi, M., Nikazar, M., Rahmani, M., and Mohamadghasemi, Z., *Chem. Eng. Res. Des.*, 2015, vol. 95, p. 239.
2. Pakhomov, N.A., Kashkin, V.N., Nemykina, E.I., Molchanov, V.V., Nadtochiy, V.I., and Noskov, A.S., *Chem. Eng. J.*, 2009, vol. 154, p. 185.
3. Shee, D. and Sayari, A., *Appl. Catal., A.*, 2010, vol. 389, p. 155.
4. Tan, S., Kim, S.-J., Moore, J.S., Liu, Y., Dixit, R.S., Pendergast, J.G., Sholl, D.S., Nair, S., and Jones, C.W., *ChemCatChem*, 2016, vol. 8, p. 214.
5. Raju, G., Reddy, B.M., and Park, S.-E., *J. CO_2 Util.*, 2014, vol. 5, p. 41.
6. Tan, S., Gil, L.B., Subramanian, N., Sholl, D.S., Nair, S., Jones, C.W., Moore, J.S., Liu, Y., Dixit, R.S., and Pendergast, J.G., *Appl. Catal., A.*, 2015, vol. 498, pp. 167–175.
7. Rodemerck, U., Sokolov, S., Stoyanova, M., Bentrup, U., Linke, D., and Kondratenko, E.V., *J. Catal.*, 2016, vol. 338, p. 174.
8. Sattler, J.J.H.B., Gonzalez-Jimenez, I.D., Luo, L., Stears, B.A., Malek, A., Barton, D.G., Kilos, B.A., Kaminsky, M.P., Verhoeven, T.W.G.M., Koers, E.J., Baldus, M., and Weckhuysen, B.M., *Angew. Chem.*, 2014, vol. 53, p. 9251.
9. Michorczyk, P., Kuśtrowski, P., Kolak, A., and Zimowska, M., *Catal. Commun.*, 2013, vol. 35, p. 95.
10. Wang, G., Sun, N., Gao, C., and Zhu, X., *Appl. Catal., A*, 2014, vol. 478, p. 71.
11. Sattler, J.J.H.B., Ruiz-Martinez, J., Santillan-Jimenez, E., and Weckhuysen, B.M., *Chem. Rev.*, 2014, vol. 114, p. 10613.
12. Hakuli, A., Kytökivi, A., and Krause, O., *Appl. Catal., A*, 1999, vol. 4827, p. 1.
13. Fang, D., Zhao, J., Li, W., Fang, X., Yang, X., Ren, W., and Zhang, H., *J. Energy Chem.*, 2015, vol. 24, p. 101.
14. Gomez Sanz, S., McMillan, L., McGregor, J., Zeitler, J.A., Al-Yassir, N., Al-Khattaf, S., and Gladden, L.F., *Catal. Sci. Technol.*, 2016, vol. 6, p. 1120.
15. Botavina, M.A., Evangelisti, C., Agafonov, Y.A., Gaidai, N.A., Panziera, N., Lapidus, A.L., and Martra, G., *Chem. Eng. J.*, 2011, vol. 166, p. 1132.
16. Michorczyk, P., Ogonowski, J., and Zenczak, K., *J. Mol. Catal. A: Chem.*, 2011, vol. 349, p. 1.
17. Sloczynski, J., Grzybowska, B., Kozlowska, A., Samson, K., Grabowski, R., Kotarba, A., and Hermanowska, M., *Catal. Today*, 2011, vol. 169, p. 29.
18. Vuurman, M.A., Wachs, I.E., Stufkens, D.J., and Oskam, A., *J. Mol. Catal.*, 1993, vol. 80, p. 209.
19. Mimura, N., Okamoto, M., Yamashita, H., Oyama, S.T., and Murata, K., *J. Phys. Chem. B*, vol. 110, p. 21764.
20. Ma, F., Chen, S., Li, Y., Zhou, H., Xu, A., and Lu, W., *Appl. Surf. Sci.*, 2014, vol. 313, p. 654.
21. Xu, L., Wang, Z., and Song, H., *Catal. Commun.*, 2013, vol. 35, p. 76.
22. Zhao, H., Song, H., and Chou, L., *Microporous Mesoporous Mater.*, 2013, vol. 181, p. 182.
23. De Rossi, S., Casaletto, M.P., Ferraris, G., Cimino, A., and Minelli, G., *Appl. Catal., A*, 1998, vol. 167, p. 257.
24. Otroshchenko, T., Radnik, J., Schneider, M., Rodemerck, U., Linke, D., and Kondratenko, E.V., *Chem. Commun.*, 2016, vol. 52, p. 8164.
25. Rezaei, M., Alavi, S.M., Sahebdelfar, S., and Yan, Z.-F., *Powder Technol.*, 2006, vol. 168, p. 59.
26. Bugrova, T.A., Litvyakova, N.N., and Mamontov, G.V., *Kinet. Catal.*, 2015, vol. 56, no. 6, p. 758.
27. Bekmukhamedov, G.E., Mukhamed'yarova, A.N., Egorova, S.R., and Lamberov, A.A., *Catalysts*, 2016, vol. 6, no. (10).
28. Neri, G., Pistone, A., De Rossi, S., Rombi, E., Milone, C., and Galvagno, S., *Appl. Catal., A*, 2004, vol. 260, p. 75.
29. Dittmar, A., Hoang, D.L., and Martin, A., *Thermochim. Acta*, 2008, vol. 470, p. 40.
30. Moriceau, P., Grzybowska, B., Gengembre, L., and Barbaux, Y., *Appl. Catal., A*, 2000, vol. 199, p. 73.
31. Martinez-Huerta, M.V., Deo, G., Luis, J., Fierro, G., and Banares, M.A., *J. Phys. Chem.*, vol. 111, p. 18708.
32. Mullins, D.R., *Surf. Sci.*, 2015, vol. 70, p. 42.
33. Wei, C., Xue, F., Miao, C., Yue, Y., Yang, W., Hua, W., and Gao, Z., Chin. J. Chem., 2017, vol. 35, p.1619.
34. Nemykina, E.I., Pakhomov, N.A., Danilevich, V.V., Rogov, V.A., Zaikovskii, V.I., Larina, T.V., and Molchanov, V.V., *Kinet. Catal.*, 2010, vol. 51, no. 6, pp. 898–906.
35. Cutrufello, M.G., De Rossi, S., Ferino, I., Monaci, R., Rombi, E., and Solinas, V., *Thermochim. Acta*, 2005, vol. 434, p. 62.
36. Cavani, F., Koutyrev, M., Trifro, F., Bartolini, A., Ghisletti, D., Iezzi, R., Santucci, A., and Del Piero, G., *J. Catal.*, 1996, vol. 158, p. 236.
37. Hardcastle, F.D. and Wachs, I.E., *J. Mol. Catal.*, 1988, vol. 46, p. 173.
38. Fridman, V.Z., Xing, R., and Severance, M., *Appl. Catal., A*, 2016, vol. 523, p. 39.